

## Proximitizing altermagnets with conventional superconductors

Niclas Heinsdorf<sup>1,2</sup> and Marcel Franz<sup>1</sup>

<sup>1</sup>*Department of Physics and Astronomy, and Quantum Matter Institute, University of British Columbia, Vancouver, British Columbia, Canada V6T 1Z1*

<sup>2</sup>*Max Planck Institute for Solid State Research, Heisenbergstrasse 1, 70569 Stuttgart, Germany*



(Received 10 September 2025; revised 2 December 2025; accepted 11 December 2025; published 6 January 2026)

Recent theoretical work highlighted the unique properties of superconducting altermagnets, including the wealth of topologically nontrivial phases as well as their potential uses in spintronic applications. Given that no intrinsically superconducting altermagnets have yet been discovered, we study here the possibility of superconducting order induced by the proximity effect from a conventional *s*-wave superconductor. Through symmetry analysis and microscopic modeling we find that interesting superconducting phases can indeed be proximity induced in a thin altermagnetic film provided that weak Rashba spin-orbit coupling is present at the interface. Surprisingly, the resulting superconductor is generically nodal with a mixed singlet/triplet order parameter and, importantly for applications, capable of generating spin-polarized persistent current. We propose a set of candidate heterostructures with low lattice mismatch suitable to probe these effects experimentally.

DOI: [10.1103/rhmg-j1fv](https://doi.org/10.1103/rhmg-j1fv)

**Introduction.** Spin-split electron bands, characteristic of metallic altermagnets [1–5], make these novel quantum materials uniquely suited for explorations into unconventional superconductivity. The key relevant observation is that, with the exception of isolated points, electrons on the Fermi surface of an altermagnet with momenta  $\mathbf{k}$  and  $-\mathbf{k}$  have the same spin  $\sigma$  and are therefore incapable of forming conventional zero-momentum spin-singlet Cooper pairs. In the presence of a weak attractive interaction the leading instability of a metallic altermagnet, then, is either a uniform equal-spin triplet order parameter [6–10], or alternately a nonzero total momentum Fulde-Ferrell-Larkin-Ovchinnikov (FFLO) state [10–12].

A discovery of either of the above superconducting (SC) phases would be rare and interesting. The triplet order parameter, for instance, requires an orbital pair wave function  $g_{\mathbf{k}}$  that is odd under inversion,  $g_{\mathbf{k}} = -g_{-\mathbf{k}}$ . In simple models a chiral *p*-wave order parameter with  $g_{\mathbf{k}} \propto (k_x \pm ik_y)$  is often energetically favored [6,7]. Such a spin-triplet chiral *p*-wave superconductor is known to be topologically nontrivial with protected chiral edge states and Majorana zero modes in vortex cores [13,14]. In addition, the specific variant likely to occur in altermagnetic (ALM) metals has two independent order parameters for two spin projections which makes it uniquely suited for the generation and transport of persistent spin currents of interest in spintronic applications [9].

Although several altermagnets that are also good metals have been discovered over the past 2 years, none so far has been reported to exhibit superconductivity. This motivates us to address the following two questions: (i) Is it possible to induce superconductivity in a metallic altermagnet by proximity effect with a conventional spin singlet *s*-wave superconductor? (ii) If so, what is the nature of the resulting SC state? These questions are nontrivial because it is not *a priori* clear how the tunneling of spin-singlet Cooper pairs might generate SC order in an altermagnet whose dominant susceptibility is towards spin-triplet pairing. We note that Ref. [15] studied

proximitized altermagnets and found numerous interesting topological phases. However, that work simply assumed that SC order would be generated and did not consider the underlying microscopic mechanism, which is of primary importance if we wish to understand conditions under which such phases might occur in realistic devices.

To address the two questions posed above we consider a setup shown in Fig. 1(a) consisting of a thin-film ALM metal supported on a substrate made of a conventional superconductor such as Pb or Al. We find that nonvanishing Rashba spin-orbit coupling (SOC) is required at the interface if one wants to generate a SC state with a gap over most of the altermagnet's Fermi surface (FS). The resulting SC state is a mixture of spin singlet and triplet orders, which is symmetry allowed in the presence broken inversion symmetry. Specifically, as indicated in Fig. 1(b), we find a proximity-induced state with portions of the FS near spin-degeneracy points

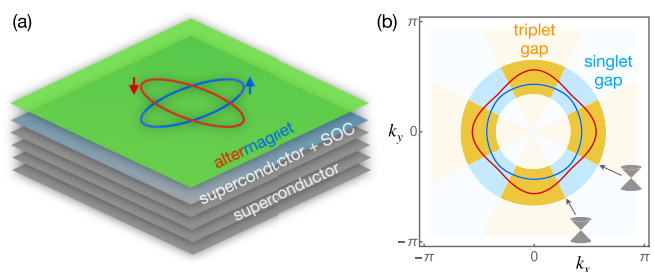


FIG. 1. (a) Sketch of the proposed setup: Altermagnetic normal metal (green) supported by a conventional *s*-wave superconductor (gray). The topmost layer of the SC substrate (blue-gray) is assumed to have Rashba SOC. (b) Schematic Fermi surface of the proximitized altermagnet. The induced Rashba SOC splits the spin degeneracy along the zone diagonals. The resulting FS is gapped out by a predominantly triplet or singlet SC order parameter as indicated, with Dirac nodal points associated with the boundaries.

gapped by a spin-singlet SC gap while the rest is dominated by a spin-triplet gap. The two types of gapped regions are separated by nodal points with Dirac quasiparticle excitations, reminiscent of nodal superconductivity found in high- $T_c$  cuprates [16]. In the minimal model of a  $d$ -wave altermagnet there are eight nodal points in the Brillouin zone (BZ), compared to four in cuprates. Nevertheless their presence leads to similar low-temperature phenomenology, including the  $T^2$  behavior of the electronic specific heat [17] and  $T$ -linear superfluid density [18,19]. Importantly, we find that parts of the FS with an induced spin-triplet SC gap are capable of supporting persistent *spin-current generation* that could be of interest for spintronic applications.

*Symmetry considerations.* At the level of phenomenological Ginzburg-Landau (GL) theory the proximity effect arises from Cooper pair tunneling from superconductor into normal metal. Mathematically this is described by a term in the GL free-energy density of the form

$$f_p[\psi_0, \psi_1] = -D(\psi_0^* \psi_1 + \text{c.c.}), \quad (1)$$

where  $\psi_{0/1}$  represent the complex scalar SC order parameters in the superconductor and normal metal, respectively. In the superconductor  $|\psi_0| > 0$ , and the linear coupling in Eq. (1) ensures that in equilibrium  $\psi_1$  will be also nonzero whenever  $D \neq 0$ . Of course  $D$  will only be nonzero when  $f_p$  is invariant under all symmetry operations. For concreteness, we focus below on a system with  $C_4$  symmetry.

When  $\psi_{0/1}$  both represent spin-singlet  $s$ -wave order parameters, then the term in Eq. (1) is allowed. On the other hand, one might think that  $D$  must necessarily vanish if we take  $\psi_1$  to represent a  $p$ -wave order parameter appropriate for the ALM normal metal. (This is because  $\psi_1$  then transforms nontrivially under  $C_4$  rotation,  $\psi_1 \rightarrow i\psi_1$ , whereas  $\psi_0 \rightarrow \psi_0$ .) However, this only describes the orbital part of the pair wave function; in order to understand the transformation properties of  $\psi_1$  we must also consider spin. As discussed in Refs. [7,9] the leading SC instability of a  $d$ -wave altermagnet occurs in four degenerate channels whose full Cooper pair wave functions can be written as

$$p_\pm^\uparrow = |\uparrow\uparrow(p_x \pm ip_y)\rangle, \quad p_\pm^\downarrow = |\downarrow\downarrow(p_x \pm ip_y)\rangle. \quad (2)$$

This expresses the simple fact that under equal-spin triplet pairing there are two possible order parameter chiralities, labeled by  $\pm$ , for each spin projection. How these order parameters transform under two-dimensional (2D) rotations depends on the  $z$  component of the total pair angular momentum  $J_z = S_z + L_z$ , where  $S_z$  and  $L_z$  denote the spin and orbital contribution, respectively. A quick thought reveals that  $p_-^\uparrow$  and  $p_+^\downarrow$  both have  $J_z = 0$  and therefore transform trivially under rotations. It follows, then, that a linear coupling shown in Eq. (1) is allowed for these two order parameters when  $\psi_0$  also transforms trivially.

Importantly, the above is true when the inversion symmetry is also broken at the surface (a  $p$  wave is odd under inversion whereas an  $s$  wave is even). In the microscopic model considered next we will account for this by including a Rashba SOC term at the SC-ALM interface which then facilitates conversion of spin-singlet to spin-triplet Cooper pairs. We conclude that, remarkably, symmetry considerations permit  $p_-^\uparrow$  and  $p_+^\downarrow$

order parameters to be proximity induced in the altermagnet from an ordinary spin-singlet  $s$ -wave superconductor.

*Microscopic model.* To understand how this occurs at the level of electron degrees of freedom, we turn to a minimal microscopic model. Specifically, we model the proximity effect in the setup depicted in Fig. 1(a) by a lattice Hamiltonian  $\mathcal{H} = \mathcal{H}_{\text{SC}} + \mathcal{H}_{\text{ALM}} + \mathcal{H}_g$  where

$$\begin{aligned} \mathcal{H}_{\text{SC}} = & \sum_{\mathbf{k}} [\xi_{\mathbf{k}} + 2\lambda_R(\sigma^x \sin k_y - \sigma^y \sin k_x)]_{\sigma\sigma'} d_{\mathbf{k}\sigma}^\dagger d_{\mathbf{k}\sigma'} \\ & + \Delta_0 \sum_{\mathbf{k}} (d_{\mathbf{k}\uparrow}^\dagger d_{-\mathbf{k}\downarrow}^\dagger + \text{H.c.}) \end{aligned} \quad (3)$$

describes the topmost layer of the SC substrate. Here,  $d_{\mathbf{k}\sigma}^\dagger$  creates an electron with momentum  $\mathbf{k}$  and spin  $\sigma$  with  $\sigma$  denoting the vector of Pauli matrices in spin space and  $\lambda_R$  the strength of Rashba SOC.  $\xi_{\mathbf{k}} = -2t(\cos k_x + \cos k_y) - \mu$  is the electron dispersion referenced to the chemical potential  $\mu$ . We note that the Rashba term is generically allowed since the inversion symmetry is necessarily broken at the surface.

The altermagnet is described by the standard  $d$ -wave model [3,4,20] on a square lattice

$$\mathcal{H}_{\text{ALM}} = \sum_{\mathbf{k}} [\xi'_{\mathbf{k}} + \sigma^z \eta_{\mathbf{k}}]_{\sigma\sigma'} c_{\mathbf{k}\sigma}^\dagger c_{\mathbf{k}\sigma'} \quad (4)$$

with the altermagnetic splitting captured by  $\eta_{\mathbf{k}} = 2\eta_0(\cos k_x - \cos k_y)$  and  $\xi'_{\mathbf{k}} = -2t'(\cos k_x + \cos k_y) - \mu'$ . The two systems are coupled by spin and momentum conserving tunneling,

$$\mathcal{H}_g = g \sum_{\mathbf{k}} (c_{\mathbf{k}\sigma}^\dagger d_{\mathbf{k}\sigma} + \text{H.c.}), \quad (5)$$

with real amplitude  $g$ . We remark that it is not difficult to enlarge the above model by, e.g., including additional SC layers or through a lattice mismatch. However, such extensions do not bring any qualitatively new features so we focus on the minimal model defined above.

It will be useful to recast the Hamiltonian  $\mathcal{H}$  in the standard Nambu matrix notation. The SC part can be written compactly as  $\mathcal{H}_{\text{SC}} = \sum_{\mathbf{k}} \Phi_{\mathbf{k}}^\dagger h_0(\mathbf{k}) \Phi_{\mathbf{k}}$  with  $\Phi_{\mathbf{k}} = (d_{\mathbf{k}\uparrow}, d_{\mathbf{k}\downarrow}, d_{-\mathbf{k}\downarrow}^\dagger, -d_{-\mathbf{k}\uparrow}^\dagger)^T$  and

$$h_0(\mathbf{k}) = \tau^z [\xi_{\mathbf{k}} + 2\lambda_R(\sigma^x \sin k_y - \sigma^y \sin k_x)] + \tau^x \Delta_0. \quad (6)$$

Here,  $\tau$  are Pauli matrices in the Nambu space. Similarly, the altermagnet can be represented as

$$h_1(\mathbf{k}) = \tau^z \xi'_{\mathbf{k}} + \sigma^z \eta_{\mathbf{k}}. \quad (7)$$

The full system is then described by an  $8 \times 8$  matrix Hamiltonian

$$H_{\mathbf{k}} = \begin{pmatrix} h_1(\mathbf{k}) & V \\ V^\dagger & h_0(\mathbf{k}) \end{pmatrix}, \quad (8)$$

with  $V = \tau^z g$ .

*Effective theory.* It is instructive to derive an effective low-energy theory for the proximitized altermagnet by formally integrating out the gapped electron degrees of freedom residing in the SC layer. This is most easily achieved by performing a unitary transformation on  $H_{\mathbf{k}}$  that renders the transformed

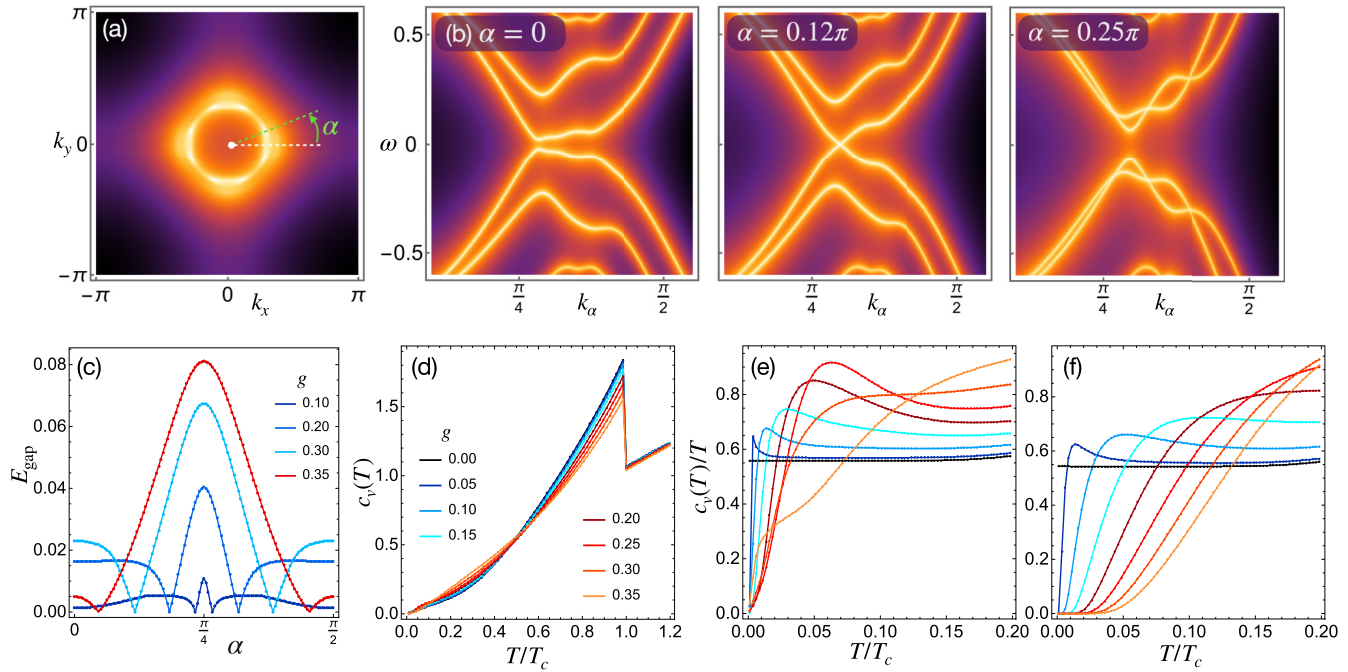


FIG. 2. Spectral properties of the proximitized altermagnet based on numerical diagonalization of Hamiltonian Eq. (8) with parameters  $(t', \mu, \mu', \eta_0, \lambda_R, \Delta_0) = (1.0, -2.80, -3.05, 0.2, 0.1, 0.4)$  and values of  $g$  as indicated, all in units of  $t$ . (a) Spectral function  $A(\mathbf{k}, \omega)$  of the altermagnetic layer at  $\omega = 0$  and  $g = 0.3$ , visualizing the underlying Fermi surface. (b)  $A(\mathbf{k}, \omega)$  along momentum space cuts  $\mathbf{k} = k_\alpha(\cos \alpha, \sin \alpha)$ . Intensities are rendered on the logarithmic scale for better clarity. (c) Excitation gap  $E_{\text{gap}}$  as a function of angle  $\alpha$ . (d) Specific heat  $c_v(T)$  as a function of temperature  $T$  and (e) detail of  $c_v(T)/T$  in the low- $T$  regime. (f) The same as (e) except in the nonmagnetic phase with  $\eta_0 = 0$ . In (d)–(f) we use an interpolation formula for the BCS gap  $\Delta(T) = \Delta_0 \tanh[1.74 \text{Re} \sqrt{T_c/T - 1}]$ , accurate over the entire range.

Hamiltonian  $\tilde{H}_k$  block diagonal. Following the steps outlined in Ref. [21], we thus obtain, to second order in coupling  $g$ ,

$$\tilde{h}_1 = h_1 - \frac{1}{2} [V h_0^{-1} V^\dagger + h_1 V h_0^{-2} V^\dagger + \text{H.c.}] + O(V^4), \quad (9)$$

where we suppressed the momentum argument to reduce clutter. The leading correction to  $h_1(\mathbf{k})$  has the form

$$\delta h_1(\mathbf{k}) = \begin{pmatrix} \Sigma_k & \Theta_k \\ \Theta_k^\dagger & -\Sigma_k \end{pmatrix}, \quad (10)$$

where  $\Sigma_k$  and  $\Theta_k$  are  $2 \times 2$  matrices in spin space.  $\Sigma_k$  represents a correction to the normal-state dispersion of the altermagnet and contains a small off-diagonal Rashba term  $\sim g^2 \lambda_R / \Delta_0^2$  that acts to resolve the spin degeneracies as indicated in Fig. 1(b). More importantly,

$$\Theta_k = \frac{g^2 \Delta_0}{\epsilon_+^2 \epsilon_-^2} \begin{pmatrix} \xi_k^2 + |\lambda_k|^2 + \Delta_0^2 & -2\xi_k \lambda_k \\ -2\xi_k \lambda_k^* & \xi_k^2 + |\lambda_k|^2 + \Delta_0^2 \end{pmatrix} \quad (11)$$

describes the SC proximity effect. Here,  $\lambda_k = 2\lambda_R(\sin k_y + i \sin k_x)$  and  $\epsilon_\pm = \sqrt{(\xi_k \pm |\lambda_k|)^2 + \Delta_0^2}$  are eigenvalues of  $h_0(\mathbf{k})$ .

Diagonal and off-diagonal elements of  $\Theta_k$  in Eq. (11) represent the spin-singlet and spin-triplet components of the pairing matrix, respectively. The latter have the correct odd-parity  $p$ -wave orbital character owing to the  $\lambda_k \sim i\lambda_R(k_x - ik_y)$  factor coming from the Rashba SOC. We also note that the proximity-induced triplet order parameter has exactly the  $p_-^\uparrow \otimes p_+^\downarrow$  structure anticipated on the basis of the symmetry analysis.

The spectrum of the effective Hamiltonian  $\tilde{h}_1 = h_1 + \delta h_1$  is analyzed in Supplemental Material (SM) [22]. We find that the singlet component of the proximity-induced order parameter, although generally larger than the triplet component, is effective in opening a gap only near the zone diagonals where the altermagnetic spin splitting is small. Elsewhere, the gap is dominated by the triplet component and the two types of the gap are separated by *nodal points* where the excitations are gapless. This gives rise to the overall gap structure displayed in Fig. 1(b). We remark that the Dirac nodes here are protected by a combination of spinfull time reversal  $\mathcal{T}$  and  $C_4$  rotation, which is a symmetry of the combined ALM-SC system; see details in SM [22].

*Numerical results.* To validate our conclusions based on the effective theory we numerically solve the full  $8 \times 8$  Hamiltonian Eq. (8); results are summarized in Fig. 2. Figures 2(a) and 2(b) show the spectral function  $A(\mathbf{k}, \omega) = -\text{Tr}' \text{Im}(\omega + i\delta - H_k)^{-1}$  of electrons in the altermagnet layer where  $\text{Tr}'$  indicates trace over the four elements pertaining to the ALM layer. Momentum cuts of  $A(\mathbf{k}, \omega)$  reveal two distinct gapped regions on the Fermi surface separated by a nodal point. In order to better visualize the proximity-induced gap we show in Fig. 2(c) the gap magnitude  $E_{\text{gap}}$  as a function of the  $k$ -space angle  $\alpha$ . This is obtained by numerically finding the smallest positive eigenvalue of  $H_k$  along the line  $\mathbf{k} = k_\alpha(\cos \alpha, \sin \alpha)$  for fixed  $\alpha$ . We observe that the nodal point lies close to the zone diagonal for small  $g$ , defining a narrow range of predominantly singlet-type gap. The gap grows in magnitude with  $g$  as the nodal points move further apart. As discussed in SM [22] this behavior can also be understood from the effective theory.

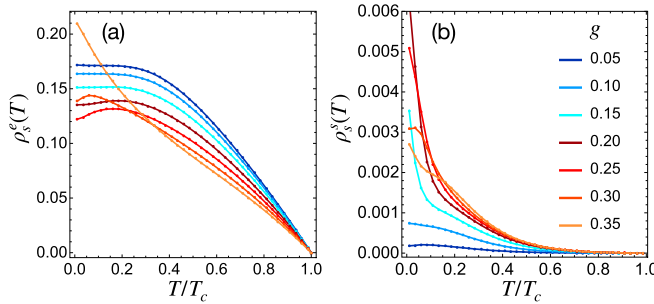


FIG. 3. Charge and spin superfluid densities of the combined bilayer system, defined in Eq. (12), plotted as a function of temperature  $T$  for the same parameters as Fig. 2.

From the knowledge of the energy eigenvalues, it is straightforward to deduce any thermodynamic quantity of interest, including the specific heat  $c_v(T)$ , which we display in Fig. 2(d). At small  $g$  and intermediate temperatures we observe a metallic  $c_v(T) \sim T$  contribution from the nearly gapless ALM layer superimposed on the exponentially activated BCS specific heat with a jump at the critical temperature  $T_c$ . The Plot of  $c_v(T)/T$  shown in Fig. 2(e) indicates a  $c_v(T) \sim T^2$  behavior at the lowest temperatures characteristic of a 2D superconductor with point nodes [16]. This contrasts with the nonmagnetic limit  $\eta_0 = 0$  shown in Fig. 2(f); in this case, the proximity effect opens up a full gap everywhere on the Fermi surface resulting in an exponentially activated  $c_v(T)$ .

*Persistent spin-current generation.* Altermagnets with intrinsic SC order have been predicted to support the spin-current dynamo effect [9], whereby charge supercurrent  $j_e$  along the zone-diagonal direction induces a pure spin supercurrent  $j_s$  with magnitude  $j_s \simeq (\eta_0/t)j_e$  along the orthogonal direction. To investigate this effect in our bilayer device we set up charge supercurrent by imposing a phase gradient  $\Delta_0 \rightarrow e^{-i\mathbf{q} \cdot \mathbf{r}}\Delta_0$  on the Hamiltonian Eq. (8) with vector  $\mathbf{q}$  along the (1, 1) direction. We then calculate expectation values of both  $j_e \parallel \mathbf{q}$  and  $j_s \perp \mathbf{q}$  and quantify the bilayer response through its charge and spin superfluid densities, defined as

$$j_e = \rho_s^e q, \quad j_s = \rho_s^s q. \quad (12)$$

The behavior of the two superfluid densities as a function of temperature  $T$  is shown in Fig. 3. For weak interlayer coupling  $g$  the charge superfluid density follows the standard BCS behavior with exponentially activated suppression  $\delta\rho_s^e(T) = \rho_s^e(T) - \rho_s^e(0)$  at low  $T$ . Increasing  $g$  initially causes a net decrease in  $\rho_s^e(T)$  magnitude which we attribute to the pair-breaking effect of the altermagnet on the superconductor (we checked that this suppression does not occur in the nonmagnetic limit  $\eta_0 = 0$ ). Eventually, at large enough  $g$ , this effect is balanced out by electrons in the altermagnet contributing to the supercurrent leading to a net increase in  $\rho_s^e(0)$ . In this regime, we also observe  $\delta\rho_s^e(T) \sim T$ , a behavior characteristic of nodal superconductors in the clean limit [18], commonly observed in  $\text{YBa}_2\text{Cu}_3\text{O}_{7-x}$  [19] and other clean high- $T_c$  cuprates [16].

Importantly, as shown in Fig. 3(b), the spin superfluid density is nonzero at low  $T$  confirming the presence of the spin-current dynamo effect. The magnitude of  $\rho_s^s$  grows as

TABLE I. Proposed heterostructures of superconductors and ALM metals with favorable low lattice mismatches along the principal axes perpendicular to the stacking direction. Crystallographic data were taken from Refs. [24–33]. Note that spin-current dynamo effects are forbidden in heterostructures with hexagonal crystal symmetry. The mismatches for the orthorhombic case correspond to the  $a$  and  $b$  axis, respectively.

SC	ALM	Mismatch	Symmetry
Al	$\text{Rb}_{1-\delta}\text{V}_2\text{Te}_2\text{O}$	0.04%	tetragonal
NbS	$\text{FeSb}_2$	0.61%, 3.21%	orthorhombic
$\text{Nb}_4\text{Se}_8$	$\text{FeBr}_3$	2.23%	hexagonal
$\text{CaKFe}_4\text{As}_4$	$\text{KV}_2\text{Se}_2\text{O}$	2.87%	tetragonal
Pb	$\text{OsO}_2$	7.64%	tetragonal

$g^2$  for small  $g$  but the growth saturates when  $g \approx \Delta_0$  and  $\rho_s^s$  never exceeds a few percent of  $\rho_s^e$ . Nevertheless  $j_s$  in this geometry represents a pure spin supercurrent which could be technologically interesting.

*Conclusions.* Contrary to the naive expectation, our results show that it is possible to induce a spin-triplet SC order parameter in a thin-film metallic altermagnet by the proximity effect from a conventional spin-singlet  $s$ -wave superconductor, provided that Rashba-type SOC is present at the interface. The resulting SC state in the altermagnet is generically nodal with eight Dirac nodes per BZ, protected by a combination of time-reversal and fourfold rotation symmetry of the system. The presence of Dirac nodes in the quasiparticle excitation spectrum can be detected directly by spectroscopic probes such as angle-resolved photoemission spectroscopy (ARPES) and scanning tunneling microscopy (STM), or through thermodynamic quantities including specific heat  $c_v(T) \sim T^2$  and superfluid density  $\delta\rho_s^e(T) \sim T$ . In addition, similar to the intrinsically superconducting altermagnets discussed theoretically [9], the proximitized altermagnet can be used to generate persistent spin current. This includes pure spin supercurrent in the geometry where the phase gradient points along the zone diagonal.

Due to its nodal structure the proximity-induced SC state in our model will exhibit flat-band edge modes similar to those found in high- $T_c$  cuprates [23]. One could also imagine starting from an ALM normal state with spin-up and spin-down Fermi pockets centered around the  $X$  and  $Y$  points of the BZ, respectively. When proximitized such a system could become fully gapped and show more conventional topology with chiral or helical edge modes.

Our conclusions follow from symmetry analysis and simple minimal models and are therefore robust and broadly applicable. Table I lists some candidate SC-ALM pairs with an in-plane antiferromagnetic ordering wave vector and closely matched lattice constants [24–33]. In particular, a heterostructure formed of aluminum and the recently discovered oxychalcogenide altermagnet  $\text{Rb}_{1-\delta}\text{V}_2\text{Te}_2\text{O}$  shows a lattice mismatch of only 0.04% and appears particularly promising [27,34].

Beyond experimental realization, several theoretical directions merit attention. These include the quantum geometry of the normal-state band structure, which has been shown to encode tendencies towards the formation of triplet super-

conductivity and altermagnetism [35,36], and the role of the interface-induced Rashba SOC and related effects tied to the charge density profile across the heterostructure, which can be studied via *ab initio* methods [37]. The “inverse proximity effect,” whereby magnetism in the ALM metal acts to suppress pairing in the SC substrate [38,39], is another important direction for future studies.

*Acknowledgments.* The authors are indebted to Yafis Barlas, Hae-Young Kee, Ivar Martin, Stuart Parkin, and Benjamin

T. Zhou for stimulating discussions and correspondence. The work was supported by Natural Sciences and Engineering Research Council of Canada, CIFAR, and the Canada First Research Excellence Fund, Quantum Materials and Future Technologies Program. M.F. thanks Aspen Center for Physics where part of this work was completed.

*Data availability.* The data that support the findings of this article are not publicly available. The data are available from the authors upon reasonable request.

- 
- [1] K.-H. Ahn, A. Hariki, K.-W. Lee, and J. Kuneš, Antiferromagnetism in RuO<sub>2</sub> as *d*-wave Pomeranchuk instability, *Phys. Rev. B* **99**, 184432 (2019).
  - [2] S. Hayami, Y. Yanagi, and H. Kusunose, Momentum-dependent spin splitting by collinear antiferromagnetic ordering, *J. Phys. Soc. Jpn.* **88**, 123702 (2019).
  - [3] L. Šmejkal, J. Sinova, and T. Jungwirth, Beyond conventional ferromagnetism and antiferromagnetism: A phase with nonrelativistic spin and crystal rotation symmetry, *Phys. Rev. X* **12**, 031042 (2022).
  - [4] L. Šmejkal, J. Sinova, and T. Jungwirth, Emerging research landscape of altermagnetism, *Phys. Rev. X* **12**, 040501 (2022).
  - [5] I. Mazin (The PRX Editors), Editorial: Altermagnetism—a new punch line of fundamental magnetism, *Phys. Rev. X* **12**, 040002 (2022).
  - [6] D. Zhu, Z.-Y. Zhuang, Z. Wu, and Z. Yan, Topological superconductivity in two-dimensional altermagnetic metals, *Phys. Rev. B* **108**, 184505 (2023).
  - [7] T. F. Heung and M. Franz, Probing topological degeneracy on a torus using superconducting altermagnets, *Phys. Rev. B* **111**, 205145 (2025).
  - [8] K. Parshukov and A. P. Schnyder, Exotic superconducting states in altermagnets, *arXiv:2507.10700*.
  - [9] K. Monkman, J. Weng, N. Heinsdorf, A. Nocera, and M. Franz, Persistent spin currents in superconducting altermagnets, *arXiv:2507.22139*.
  - [10] S. Hong, M. J. Park, and K.-M. Kim, Unconventional *p*-wave and finite-momentum superconductivity induced by altermagnetism through the formation of Bogoliubov Fermi surface, *Phys. Rev. B* **111**, 054501 (2025).
  - [11] S. Sumita, M. Naka, and H. Seo, Fulde-Ferrell-Larkin-Ovchinnikov state induced by antiferromagnetic order in  $\kappa$ -type organic conductors, *Phys. Rev. Res.* **5**, 043171 (2023).
  - [12] D. Chakraborty and A. M. Black-Schaffer, Zero-field finite-momentum and field-induced superconductivity in altermagnets, *arXiv:2309.14427*.
  - [13] N. Read and D. Green, Paired states of fermions in two dimensions with breaking of parity and time-reversal symmetries and the fractional quantum Hall effect, *Phys. Rev. B* **61**, 10267 (2000).
  - [14] L. Fu and C. L. Kane, Superconducting proximity effect and Majorana fermions at the surface of a topological insulator, *Phys. Rev. Lett.* **100**, 096407 (2008).
  - [15] Sayed Ali Akbar Ghorashi, T. L. Hughes, and J. Cano, Altermagnetic routes to Majorana modes in zero net magnetization, *Phys. Rev. Lett.* **133**, 106601 (2024).
  - [16] C. C. Tsuei and J. R. Kirtley, Pairing symmetry in cuprate superconductors, *Rev. Mod. Phys.* **72**, 969 (2000).
  - [17] K. A. Moler, D. J. Baar, J. S. Urbach, R. Liang, W. N. Hardy, and A. Kapitulnik, Magnetic field dependence of the density of states of YBa<sub>2</sub>Cu<sub>3</sub>O<sub>6.95</sub> as determined from the specific heat, *Phys. Rev. Lett.* **73**, 2744 (1994).
  - [18] J. Annett, N. Goldenfeld, and S. R. Renn, Interpretation of the temperature dependence of the electromagnetic penetration depth in YBa<sub>2</sub>Cu<sub>3</sub>O<sub>7- $\delta$</sub> , *Phys. Rev. B* **43**, 2778 (1991).
  - [19] W. N. Hardy, D. A. Bonn, D. C. Morgan, R. Liang, and K. Zhang, Precision measurements of the temperature dependence of  $\lambda$  in YBa<sub>2</sub>Cu<sub>3</sub>O<sub>6.95</sub>: Strong evidence for nodes in the gap function, *Phys. Rev. Lett.* **70**, 3999 (1993).
  - [20] M. Roig, A. Kreisel, Y. Yu, B. M. Andersen, and D. F. Agterberg, Minimal models for altermagnetism, *Phys. Rev. B* **110**, 144412 (2024).
  - [21] Y. Yao, F. Ye, X.-L. Qi, S.-C. Zhang, and Z. Fang, Spin-orbit gap of graphene: First-principles calculations, *Phys. Rev. B* **75**, 041401(R) (2007).
  - [22] See Supplemental Material at <http://link.aps.org/supplemental/10.1103/rhmg-j1fv> for analysis of the effective Hamiltonian spectrum, stability of Dirac nodes and the importance of Rashba spin-orbit coupling.
  - [23] F. Wang and D.-H. Lee, Topological relation between bulk gap nodes and surface bound states: Application to iron-based superconductors, *Phys. Rev. B* **86**, 094512 (2012).
  - [24] A. Jain, S. P. Ong, G. Hautier, W. Chen, W. D. Richards, S. Dacek, S. Cholia, D. Gunter, D. Skinner, G. Ceder, and K. A. Persson, Commentary: The materials project: A materials genome approach to accelerating materials innovation, *APL Mater.* **1**, 011002 (2013).
  - [25] S. Hastrup, M. Strange, M. Pandey, T. Deilmann, P. S. Schmidt, N. F. Hinsche, M. N. Gjerding, D. Torelli, P. M. Larsen, A. C. Riis-Jensen, *et al.*, The computational 2D materials database: High-throughput modeling and discovery of atomically thin crystals, *2D Mater.* **5**, 042002 (2018).
  - [26] M. N. Gjerding, A. Taghizadeh, A. Rasmussen, S. Ali, F. Bertoldo, T. Deilmann, N. R. Knøsgaard, M. Kruse, A. H. Larsen, S. Manti, *et al.*, Recent progress of the computational 2D materials database (C2DB), *2D Mater.* **8**, 044002 (2021).
  - [27] A. Abilim, Y.-L. Sun, H. Jiang, S.-Q. Wu, Y.-B. Liu, and G.-H. Cao, Weak metal-metal transition in the vanadium oxytelluride Rb<sub>1- $\delta$</sub> V<sub>2</sub>Te<sub>2</sub>O, *Phys. Rev. B* **97**, 214517 (2018).
  - [28] J. Sødequist and T. Olsen, Two-dimensional altermagnets from high throughput computational screening: Symmetry require-

- ments, chiral magnons, and spin-orbit effects, *Appl. Phys. Lett.* **124**, 182409 (2024).
- [29] N. Heinsdorf, M. H. Christensen, M. Iraola, S.-S. Zhang, F. Yang, T. Birol, C. D. Batista, R. Valentí, and R. M. Fernandes, Prediction of double-Weyl points in the iron-based superconductor Ca K Fe<sub>4</sub> As<sub>4</sub>, *Phys. Rev. B* **104**, 075101 (2021).
- [30] Y. Xu, H. Zhang, M. Feng, and F. Tian, Electronic structure, magnetic transition, and Fermi surface instability of the room-temperature altermagnet KV<sub>2</sub>Se<sub>2</sub>O, *Phys. Rev. B* **112**, 125141 (2025).
- [31] P. R. Raghuvanshi, T. Berlijn, D. S. Parker, S. Wang, M. E. Manley, R. P. Hermann, L. Lindsay, and V. R. Cooper, Altermagnetic behavior in OSo<sub>2</sub>: Parallels with RuO<sub>2</sub>, *Phys. Rev. Mater.* **9**, 034407 (2025).
- [32] I. I. Mazin, K. Koepernik, M. D. Johannes, R. González-Hernández, and L. Šmejkal, Prediction of unconventional magnetism in doped FeSb<sub>2</sub>, *Proc. Natl. Acad. Sci. USA* **118**, e2108924118 (2021).
- [33] B.-B. Ruan, J.-K. Yi, L.-W. Chen, M. Zhou, Y.-Q. Shi, Q.-S. Yang, Y.-D. Gu, G.-F. Chen, and Z.-A. Ren, Superconductivity in orthorhombic NbS, *Phys. Rev. B* **108**, 174517 (2023).
- [34] F. Zhang, X. Cheng, Z. Yin, C. Liu, L. Deng, Y. Qiao, Z. Shi, S. Zhang, J. Lin, Z. Liu, M. Ye, Y. Huang, X. Meng, C. Zhang, T. Okuda, K. Shimada, S. Cui, Y. Zhao, G.-H. Cao, S. Qiao, *et al.*, Crystal-symmetry-paired spin-valley locking in a layered room-temperature antiferromagnet, *Nat. Phys.* **21**, 760 (2025).
- [35] T. Kitamura, A. Daido, and Y. Yanase, Spin-triplet superconductivity from quantum-geometry-induced ferromagnetic fluctuation, *Phys. Rev. Lett.* **132**, 036001 (2024).
- [36] N. Heinsdorf, Altermagnetic instabilities from quantum geometry, *Phys. Rev. B* **111**, 174407 (2025).
- [37] Q.-F. Yao, J. Cai, W.-Y. Tong, S.-J. Gong, J.-Q. Wang, X. Wan, C.-G. Duan, and J. H. Chu, Manipulation of the large rashba spin splitting in polar two-dimensional transition-metal dichalcogenides, *Phys. Rev. B* **95**, 165401 (2017).
- [38] S.-B. Zhang and L.-H. Hu, Finite-momentum mixed singlet-triplet pairing in chiral antiferromagnets induced by even-parity spin texture, arXiv:2507.20549.
- [39] S.-B. Zhang, L.-H. Hu, Q. Niu, and Z. Zhang, Spin-valley locking and pure spin-triplet superconductivity in noncollinear antiferromagnets proximitized to conventional superconductors, arXiv:2507.11921.